J Mater Sci (2007) 42:8558–8570
DOI 10.1007/s10853-007-1810-8

Effect of Al_2O_3 concentration on zirconolite ($Ca(Zr,Hf)Ti_2O_7$) crystallization in (TiO_2,ZrO_2,HfO_2)-rich SiO_2–Al_2O_3–CaO–Na_2O glasses

Daniel Caurant · Pascal Loiseau · Isabelle Bardez · Christel Gervais

Received: 7 February 2007 / Accepted: 27 April 2007 / Published online: 9 July 2007

Abstract Glass-ceramic matrices containing zirconolite (nominally $Ca(Zr,Hf)Ti_2O_7$) crystals in their bulk that would incorporate high proportions of minor actinides (Np, Am, Cm) or plutonium could be envisaged for their immobilization. Zirconolite-based glass-ceramics can be prepared by controlled crystallization of zirconolite in glasses belonging to SiO_2–Al_2O_3–CaO–Na_2O–TiO_2–ZrO_2–HfO_2 system. In this study, neodymium was used as trivalent actinides surrogate. Increasing Al_2O_3 concentration in glass composition had a strong effect on the nucleation rate I_z of zirconolite crystals in the bulk, on the amount of neodymium incorporated in zirconolite phase and on the crystal growth rate of silicate phases (titanite + anorthite) from glass surface. These results could be explained by the existence of competition—in favor of aluminum—between Al^{3+} and (Ti^{4+}, Zr^{4+}, Hf^{4+}) ions for their association with charge compensators cations to facilitate their incorporation in the glassy network. Differential thermal analysis (DTA) was used to study exothermal effects associated with bulk and surface crystallization. ^{27}Al magic angle spinning nuclear magnetic resonance (MAS NMR) spectra showed that aluminum enters glasses network predominantly in 4-fold coordination. Neodymium optical absorption and fluorescence spectroscopies showed that the Al_2O_3 concentration changes performed in this study had not significant effect on Nd^{3+} ions environment in glasses.

D. Caurant (✉) · P. Loiseau · I. Bardez
Laboratoire de Chimie de la Matière Condensée de Paris, UMR-CNRS 7574, Ecole Nationale Supérieure de Chimie de Paris (ENSCP, ParisTech), 11 rue Pierre et Marie Curie, Paris 75231, France
e-mail: daniel-caurant@enscp.fr

C. Gervais
Laboratoire de Chimie de la Matière Condensée de Paris, UMR-CNRS 7574, Université Pierre et Marie Curie, 4 Place Jussieu, Paris 75252, France

Introduction

Currently, borosilicate and phosphate glasses are the only waste forms used industrially (France, Russia, United States, Great Britain...) for the immobilization of highly radioactive nuclear wastes (HLW) [1–4]. Such wastes are generated after the reprocessing of spent nuclear fuel used in power (electricity production) or military (Pu production) reactors. In these wastes, inactive elements and short-lived, medium-lived or long-lived radionuclides are mixed together and the waste form matrices must incorporate simultaneously all of them [4, 5]. Because of this chemical complexity and also because of the occurrence of high amounts of volatile elements (Cs, Ru...) in HLW solutions, glasses that can be melted at low temperature (1100–1150 °C) have been chosen as waste forms. Indeed, glassy matrices distinguish themselves from crystalline matrices by the very wide range of solid solutions, which is due to the lack of long-range ordering in their structure. This allows the accommodation in various proportions within the glassy network of a great variety of elements with their own chemical bonding requirements and thus glasses are able to incorporate high quantities of the different elements occurring in HLW. However, because of the introduction of significant Na_2O and B_2O_3 concentrations in nuclear borosilicate compositions [3, 4] to enable their melting at low temperature, the chemical durability of these waste forms is not as good as the one that can be reached for more refractory glasses such as aluminosilicate glasses.

Nevertheless, the selective separation of several long-lived radionuclides (such as minor actinides, cesium and technetium) from HLW followed by their immobilization in highly durable specific titanate, zirconate or phosphate ceramic matrices [3, 4, 6–9] more durable than the nuclear glasses currently used industrially, could be envisaged in several countries such as France [10, 11] and Russia [12, 13]. Among these long-lived radionuclides, minor actinides (Np, Am, Cm) represent the main contribution to the long-term potential radiotoxicity of nuclear wastes [14]. The same problem of immobilization also exists for excess plutonium from dismantled nuclear weapons (Russia, United States). For the immobilization of actinides, the studies reported in literature concern mainly ceramic waste forms (zirconolite, pyrochlore, apatite, monazite) [6–8, 15, 16]. However, due to the facility of glass preparation by melting + casting, glass-ceramics could be envisaged as interesting alternative waste forms [4]. Indeed, such matrices that can be obtained by controlled crystallization of a highly durable phase (able to incorporate minor actinides and Pu) either during cooling of melts or after reheating of parent glasses, would accept more easily waste composition fluctuations than ceramics. Moreover, the minor actinides incorporated in the highly durable crystalline phase in the bulk of the glass-ceramics would benefit of a double containment barrier (crystal + glass). In previous works, we reported the possibility to prepare zirconolite-based glass-ceramics by controlled crystallization (nucleation + crystal growth) of parent glasses belonging to the SiO_2–Al_2O_3–CaO–Na_2O–TiO_2–HfO_2–ZrO_2–Ln_2O_3 (Ln: lanthanide) system [17–22]. In these studies, trivalent lanthanides (mainly Nd^{3+}) were used to simulate trivalent minor actinides (Am^{3+}, Cm^{3+}) [23]. In this system, zirconolite (nominally $Ca(Zr,Hf)Ti_2O_7$) was found to be the only crystalline phase to nucleate in the bulk whereas titanite and anorthite crystals (nominally $CaTiSiO_5$ and $CaAlSi_2O_8$) nucleated heterogeneously on glass surface. Zirconolite is a highly durable crystalline phase well known for its capacity to incorporate high amounts of actinides and lanthanides [24–28] and for its excellent leaching resistance [29–30] even after amorphization induced by radiation damage [31]. The structure of zirconolite is described for instance in [24, 32]. Several effects of parent glass composition changes (TiO_2, ZrO_2, CaO and Ln_2O_3 concentrations) on glass crystallization (surface + bulk) and on the proportion of lanthanides incorporated in the crystalline phases were already reported. For instance, surface and bulk crystallization was studied using differential thermal analysis (DTA) and X-ray diffraction (XRD) for glasses with increasing TiO_2 and ZrO_2 concentrations [33]. The effect of partial or total substitution of ZrO_2 by HfO_2 on glass crystallization and more particularly on the nucleation rate and the composition of zirconolite crystals was also studied because hafnium has a high thermal neutron capture cross-section in comparison with zirconium [22, 34]. In this case, the occurrence of hafnium—acting as neutron poison for fission reactions—in zirconolite crystals may prevent criticality events in glass-ceramics waste forms heavily loaded with fissile actinide isotopes such as ^{239}Pu.

In previous works [23, 35], we showed that Al^{3+} ions partly insured Ln^{3+} ions charge compensation in the zirconolite crystals growing in the bulk of the glass-ceramics. Thus, the occurrence of Al_2O_3 in parent glass composition helps trivalent minor actinide and plutonium surrogate incorporation into the zirconolite phase. Moreover, Ln^{3+} ions were also shown to be incorporated into the titanite crystals growing from glass surface. In this case, Al^{3+} ions also insured charge compensation in the crystals [18, 21].

In this paper, we study the effect of Al_2O_3 concentration change in parent glasses composition containing either zirconium or hafnium on their crystallization behavior both in the bulk and from the surface. The nature, the microstructure and the nucleation rate of phases crystallizing in these glasses are studied. As it is shown, alumina has a strong effect both on the zirconolite nucleation rate I_Z in the bulk and on the total amount of Nd^{3+} ions incorporated in zirconolite. Considerations about both the structural role of Al^{3+} ions and the existence of a competition between Al^{3+} and (Ti^{4+}, Zr^{4+}, Hf^{4+}) ions for association with charge compensators in glass and melt structure are developed to explain these results. To complete this crystallization study, the environment of Nd^{3+} and Al^{4+} ions in parent glasses was studied respectively by optical spectroscopy and MAS NMR.

Experimental procedures

Six glasses belonging to SiO_2–Al_2O_3–CaO–Na_2O–TiO_2–ZrO_2–HfO_2 system were prepared for this study according to the method described in [17]. The target glass compositions are given in Table 1. The composition of several glass samples determined by the inductively coupled plasma-atomic emission spectrometry (ICP-AES) method or by electron probe microanalysis (EPMA) are also given in this Table. Two kinds of glasses can be distinguished: glasses with ZrO_2 ($GZr(Nd)_a$,$GZr(Nd)_b$,$GZr(Nd)_c$,GZr) and glasses with HfO_2 ($GHf(Nd)_a$,$GHf(Nd)_c$). $GZr(Nd)_a$, GZr and $GHf(Nd)_a$ correspond to compositions already studied in previous works [17–19]. The other compositions of Table 1 were deduced from $GZr(Nd)_a$ and $GHf(Nd)_a$ compositions either increasing ($GZr(Nd)_c$,$GHf(Nd)_c$) or decreasing ($GZr(Nd)_b$) Al_2O_3 concentration by respectively 2.6 and 2.8 mol% keeping constant the relative concentrations of other oxides except Nd_2O_3. As in our previous

Table 1 Composition (in weight and molar percentages) of parent glasses leading to zirconolite crystallization in their bulk

Glass reference	Composition	SiO_2	Al_2O_3	CaO	TiO_2	ZrO_2	HfO_2	Nd_2O_3	Na_2O	T_g (°C)
$GZr(Nd)_a$	wt%[a]	40.57	11.94	19.63	12.45	8.46	0.00	6.00	0.94	761 ± 2
	wt%[b]	40.64	12.32	20.06	12.02	8.03	0.00	5.92	1.01	
	wt%[c]	39.11	11.94	20.02	12.67	9.13	0.01	6.29	0.81	
	mol%[a]	48.23	8.37	25.00	11.14	4.90	0.00	1.27	1.08	
$GZr(Nd)_b$	wt%[a]	42.48	8.08	20.55	13.04	8.86	0.00	6.00	0.98	
	mol%[a]	49.73	5.57	25.78	11.48	5.06	0.00	1.25	1.11	
$GZr(Nd)_c$	wt%[a]	38.83	15.48	18.78	11.92	8.10	0.00	6.00	0.90	760 ± 2
	mol%[a]	46.81	11.00	24.27	10.81	4.76	0.00	1.29	1.05	
$GHf(Nd)_a$	wt%[a]	38.27	11.27	18.52	11.75	0.00	13.64	5.66	0.89	765 ± 2
	wt%[c]	38.17	10.97	18.84	11.82	0.09	13.49	5.77	0.83	
	mol%[a]	48.23	8.37	25.00	11.14	0.00	4.91	1.27	1.08	
$GHf(Nd)_c$	wt%[a]	36.71	14.64	17.77	11.27	0.00	13.08	5.67	0.85	
	mol%[a]	46.81	11.00	24.27	10.81	0.00	4.76	1.29	1.05	
GZr	wt%[a]	43.15	12.71	20.88	13.25	9.00	0.00	0.00	1.00	760 ± 2
	wt%[b]	42.75	12.62	21.20	13.49	8.90	0.00	0.00	1.04	
	mol%[a]	48.85	8.48	25.33	11.28	4.97	0.00	0.00	1.10	

[a] Target compositions

[b] Composition analyzed by ICP-AES (estimated error ± 2–5 wt%)

[c] Composition analyzed by EPMA. The glass transformation temperature T_g—determined by DTA using the onset of the corresponding endothermic effect—is also given for several samples. A small amount of Na_2O ($[Na_2O] \leq 1$ wt%) was introduced as tracer element in all glass compositions in order to perform chemical durability tests on both parent glasses and glass-ceramics that are not presented in this paper

studies, neodymium was used as trivalent minor actinides and plutonium surrogate: 6 and 5.6 wt% Nd_2O_3 (corresponding to nearly 1.3 mol%) were introduced in glass compositions containing respectively ZrO_2 and HfO_2. This Nd_2O_3 concentration corresponds approximately to 9.2 wt% Am_2O_3 for glasses containing zirconium if all neodymium ions are replaced by americium ions. The choice of lower Nd_2O_3 concentration (5.6 wt%) for glasses containing hafnium was made in order to keep nearly the same molar concentration of Nd_2O_3 in $GZr(Nd)_x$ and $GHf(Nd)_x$ (x = a, c) samples. Composition GZr is similar to composition $GZr(Nd)_a$ but without Nd_2O_3. For all glass compositions, a small amount of Na_2O ($[Na_2O] \sim 1$ mol%) was introduced as tracer element to perform chemical durability tests that are not presented in this paper. Thus, even if a small fraction of the negatively charged polyhedra (such as $(AlO_4)^-$) of the glassy network can be charge compensated by Na^+ ions, Ca^{2+} ions are the main charge compensators for the glass compositions studied in this paper ($[Na_2O]/[CaO] = 0.04$ in mol%, Table 1).

Glasses of Table 1 were prepared using reagent-grade SiO_2, Al_2O_3, $CaCO_3$, TiO_2, ZrO_2, HfO_2, Na_2CO_3 and Nd_2O_3 raw materials. Batches (50 g) were melted in platinum crucibles and refined at 1550 °C. Because of the lack of mechanical mixing during melting, a two-step melting was performed with an intermediate grinding stage to obtain homogeneous glasses [18, 23]. After casting cylinders in steel molds (10 mm high and 14 mm diameter), all glass samples were annealed at T = 775 °C for 2 h in order to relieve strains before cutting. This annealing temperature was slightly higher than the glass transformation temperature T_g (Table 1). Glass-ceramics were then prepared following a two-step heat treatment: nucleation (T_n = 810 °C, 2 h) and crystal growth (T_c = 1050 °C or 1200 °C, 2 h) [17, 18]. After nucleation, the samples were immediately transferred into a furnace preheated at T_c. After crystal growth, the glass-ceramic samples were directly annealed at 775 °C for 2 h before slow cooling to room temperature. The nucleation rate curves $I_z = f(T)$ of zirconolite in $GZr(Nd)_a$ glass and in a glass whose composition was similar to the one of $GHf(Nd)_a$ but without neodymium were reported in [34]. The crystal growth temperatures T_c chosen here (1050 and 1200 °C) were shown to lead to the crystallization of only zirconolite in the bulk of $GZr(Nd)_a$ and $GHf(Nd)_a$ samples [17].

Several glass samples were characterized (glass transformation and crystallization peak temperatures) using differential thermal analysis (DTA) with the help of a NETZSCH STA 409 thermal analysis apparatus (heating rate at 10 °C min^{-1} under air in platinum crucibles, glass particle size 125–250 μm). Ignited alumina was used as reference material. For $GZr(Nd)_c$, the quenched glass was crushed and sieved to obtain four size fractions (<20, 40–80, 125–200, 1600–2000 μm). DTA runs were then

performed for these different size fractions in order to follow the evolution (displacement and intensity) of exothermal peaks associated with crystallization.

In order to study the structural role of aluminum in our glasses, ^{27}Al (I = 5/2, natural abundance 100%) solid-state magic angle spinning nuclear magnetic resonance (MAS NMR) spectra were recorded for GZr and GZr(Nd)$_a$ glasses using a Bruker DRX600 liquid spectrometer (14.1 T) operating at 156.38 MHz and equipped with a Bruker high speed MAS probe-head (2.5 mm zirconia rotors) spinning at 26 kHz. Small pulse flip angles ($<\pi/12$) were applied thus enabling a linear regime excitation for the spin system [36]. Chemical shifts were referenced to an acidic aqueous solution of $Al(NO_3)_3$ (1 M) and 2500 scans were accumulated. In order to confirm the coordination state of Al^{3+} ions determined by MAS NMR in the glassy network without being disturbed by broadening due to second order quadrupolar effect, the ^{27}Al triple quantum 3QMAS NMR spectrum of GZr glass (sample without paramagnetic Nd^{3+} ions) was also recorded.

Neodymium optical absorption and fluorescence spectra were recorded for GZr(Nd)$_a$, GZr(Nd)$_b$, GZr(Nd)$_c$ and GHf(Nd)$_a$ glasses. Fluorescence decay curves were recorded for GZr(Nd)$_a$, GZr(Nd)$_b$ and GZr(Nd)$_c$ glasses. A Varian Cary 5E double beam spectrometer was used to record optical absorption spectra at $T < 15$ K. Fluorescence decays $I = f(t)$ (I being the emitted intensity) were recorded at 300 K following $^4F_{3/2} \rightarrow {}^4I_{11/2}$ neodymium transition (near 1062 nm) with a InGaAs detector after non-selective excitation near 585 nm (corresponding to the strong $^4I_{9/2} \rightarrow {}^4G_{5/2},{}^2G_{7/2}$ transition of neodymium, Fig. 1) with an optical parametric oscillator pumped by the third harmonic of a pulsed Nd-YAG laser. As excitation is non selective, we can assume that if Nd^{3+} ions are located in different environments in the glass structure, they will be all excited after the laser pulse. As fluorescence decay curves are not exponential for the samples studied in this work (Fig. 2), the mean lifetime τ_m of excited Nd^{3+} ions was estimated by integration using the following formula:

$$\tau_m = (1/I_0)\int I(t)dt \quad (1)$$

where I_0 is the emitted intensity when $t = 0$.

Glass-ceramic samples were characterized using different techniques. Powder X-ray diffraction (XRD) patterns were recorded with the help of a Siemens D5000 instrument with CoK_α radiation (λ= 1.78897 Å). Scanning electron microscopy (SEM) and energy dispersive X-ray analysis (EDX) of crystals were performed at 15 kV on polished and carbon coated glass-ceramic samples with a Hitachi S2500 microscope and a PGT EDX analyzer. For GHf(Nd)$_a$ glass-ceramic sample, the composition of zirconolite crystals was determined by electron probe microanalysis (EPMA). Electron spin resonance (ESR) was used to follow the incorporation neodymium and to estimate the amount of Nd^{3+} ions ($4f^3$) in the zirconolite crystals of the glass-ceramics. The method used for this estimation was described in [37]. The spectra were recorded at 12 K using a Bruker ESP 300e ESR spectrometer operating at X-band ($\nu \sim 9.5$ GHz).

Results and discussion

As cast samples were all fully transparent and X-ray amorphous. The composition of GZr(Nd)$_a$, GHf(Nd)$_a$ and GZr glasses was analyzed by ICP-AES and/or EPMA. As the analyzed and target compositions are very similar for these three samples (Table 1), we can expect that it is also the case for GZr(Nd)$_b$, GZr(Nd)$_c$ and GHf(Nd)$_c$ glasses because of the lack of significant amount of volatile

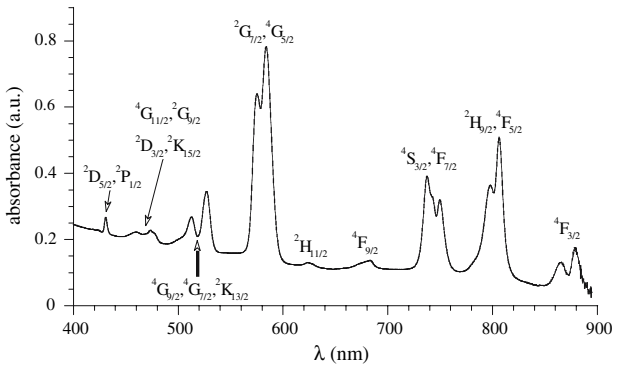

Fig. 1 Optical absorption spectrum of GZr(Nd)$_a$ glass ($T < 15$ K). The neodymium excited states corresponding to the different transitions from the fundamental $^4I_{9/2}$ state are indicated in the figure

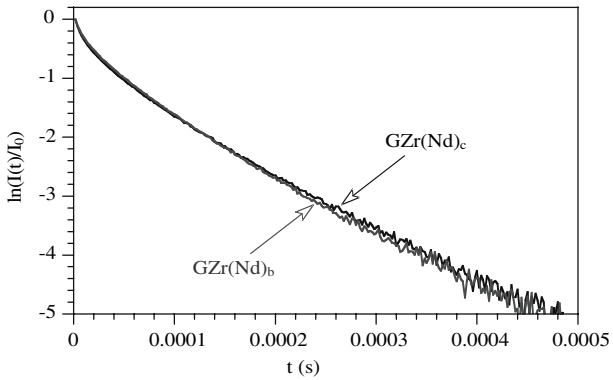

Fig. 2 Comparison of Nd^{3+} ions fluorescence decay curves (T = 300 K) in GZr(Nd)$_b$ and GZr(Nd)$_c$ glasses. Excitation at 585 nm ($^4I_{9/2} \rightarrow {}^4G_{5/2},{}^2G_{7/2}$ transition) and emission at 1062 nm ($^4F_{3/2} \rightarrow {}^4I_{11/2}$ transition). I_0: intensity emitted at time $t = 0$. I(t): intensity emitted at time t

element such as sodium ([Na_2O] ≤ 1 wt%) in these compositions. The glass transformation temperatures reported in Table 1 show that the composition changes performed in this study have not significant impact on T_g.

Structural study of parent glasses

Optical absorption and fluorescence study of neodymium

Optical absorption spectra of $GZr(Nd)_a$, $GZr(Nd)_b$ and $GZr(Nd)_c$ glasses are very similar. For instance, the spectrum of $GZr(Nd)_a$ sample is shown in Fig. 1. According to literature results about neodymium optical absorption in oxide glasses [38–42], the lack of shoulders on the low energy side of the two main peaks of the $^4I_{9/2} \rightarrow {}^4G_{5/2}$, $^2G_{7/2}$ transition (Fig. 1) indicates that Nd^{3+} ions are located either in depolymerized regions of the glassy network (i.e. in regions containing high concentration of non-bridging oxygen atoms (NBO)) in association with high field strength modifier cations (Ca^{2+} in this study) or in polymerized regions of the glassy network. As shown below, the amount of modifier cations available to form NBO is low for the glasses studied in this work, which could indicate that neodymium is mainly located in polymerized regions. Nevertheless, because of the small Nd_2O_3 concentration (~1.3 mol%, Table 1) it is difficult to rule out the possibility that a high proportion of neodymium ions occurring in these glasses are located near NBO and Ca_{2+} ions in depolymerized regions. Indeed, it is known that in oxide glasses, Nd^{3+} ions are preferentially located in NBO rich regions of the glassy network [39]. The position of the $^4I_{9/2} \rightarrow {}^2P_{1/2}$ (~431 nm) and $^4I_{9/2} \rightarrow {}^4F_{3/2}$ (~865–879 nm) absorption bands of neodymium moves only of about 3 cm^{-1} between the three glasses which is negligible. As the position of neodymium absorption bands is known to be sensitive both to crystal field symmetry and to the distance between Nd^{3+} ions and their first neighbors (oxygen ions) [38–42], these spectroscopic results show that Nd^{3+} ions environment in $GZr(Nd)_x$ glasses ($x = a, b, c$) does not significantly vary when Al_2O_3 concentration increases. Moreover, neodymium fluorescence decay curves are nearly identical for the three glasses. For instance, the decay curves of $GZr(Nd)_b$ and $GZr(Nd)_c$ glasses are shown in Fig. 2. The mean lifetime τ_m of the $^4F_{3/2}$ excited state of neodymium deduced from the decay curves is estimated at 60 μs ± 1 μs for these three samples. Contrary to the results obtained in [22] for a sample with composition similar to that of $GZr(Nd)_a$ glass but containing only 0.5 wt% Nd_2O_3 and that showed an almost exponential decay curve (with τ_m ~ 295 μs), the fluorescence decays of $GZr(Nd)_x$ ($x = a, b, c$) glasses are not exponential. The evolution of decay curves and the decrease of τ_m between these three glasses and the glass containing 0.5 wt% Nd_2O_3 [22] indicates the existence of interactions between Nd^{3+} ions for the samples containing 6 wt% Nd_2O_3. Such interactions induce energy transfer between Nd^{3+} ions followed by energy transfer on a quenching site and/or cross relaxation between Nd^{3+} ions followed by non-radiative decay [22, 43]. Thus, the decrease of τ_m when [Nd_2O_3] increases from 0.5 to 6 wt% can be explained by a decrease of the average distance between Nd^{3+} ions in the glass structure. At low neodymium concentration an exponential $I = f(t)$ decay is obtained because the distance between Nd^{3+} ions is so large that no significant energy transfer occurs. The fact that Nd^{3+} ions fluorescence decay curves do not change between $GZr(Nd)_b$ and $GZr(Nd)_c$ glasses indicates that increasing Al_2O_3 concentration from 5.57 to 11.00 mol% has no significant effect on non-radiative disexcitation of neodymium. This means that the composition changes performed in this study do not significantly modify the interactions and the average distance between neodymium ions in the glassy network.

The similarity of optical absorption and fluorescence spectra of $GZr(Nd)_a$ and $GHf(Nd)_a$ glasses (spectra not shown) shows that the total substitution of zirconium by hafnium in glass composition has not significant effect on the environment of Nd^{3+} ions in glass structure. Study of $GZr(Nd)_a$ and $GHf(Nd)_a$ glasses by ESR confirms that neodymium ions environment is not significantly affected by this substitution [22]. These results can be explained by the very similar chemical properties of Zr^{4+} and Hf^{4+} ions and consequently by their very similar structural role in glass structure. Indeed, EXAFS results published on aluminoborosilicate nuclear glasses containing either ZrO_2 [44] or HfO_2 [45] showed that Zr^{4+} and Hf^{4+} ions both occurred in 6-fold coordinated sites with distances d(Zr–O) = 2.08 Å and d(Hf–O) = 2.07 Å respectively. Moreover, our results about neodymium in $GZr(Nd)_a$ and $GHf(Nd)_a$ parent glasses are also in accordance with other results we obtained for neodymium in $Ca_{0.8}Nd_{0.2}ZrTi_{1.8}Al_{0.2}O_7$ and $Ca_{0.8}Nd_{0.2}HfTi_{1.8}Al_{0.2}O_7$ zirconolite ceramics for which no significant effect of total replacement of zirconium by hafnium was observed on Nd^{3+} ions optical absorption and fluorescence spectra [22].

^{27}Al MAS NMR study

^{27}Al MAS NMR spectra were recorded for GZr and $GZr(Nd)_a$ glasses to elucidate the role of aluminum ions in glass structure. The spectrum of GZr glass without neodymium (Fig. 3a) shows an intense resonance with isotropic chemical shift δ_{iso} around 60 ppm indicative of Al in tetrahedral coordination with oxygen atoms [46–49]. No features can be clearly identified in the spectral regions assigned to 5-fold and 6-fold coordination (δ_{iso} = +25 to +40 ppm and –15 to +20 ppm, respectively). The peak is

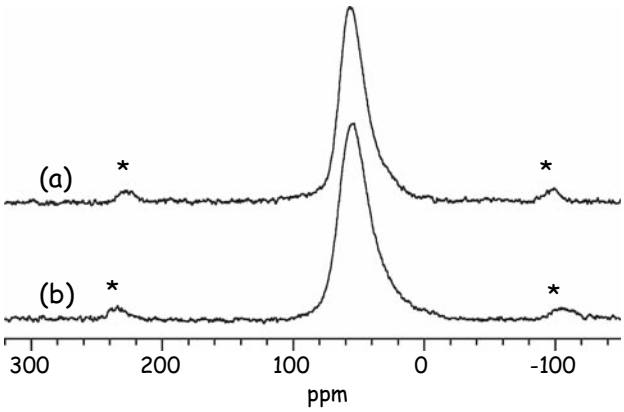

Fig. 3 ^{27}Al MAS NMR spectra of GZr (**a**) and GZr(Nd)$_a$ (**b**) glasses (* indicates spinning sidebands)

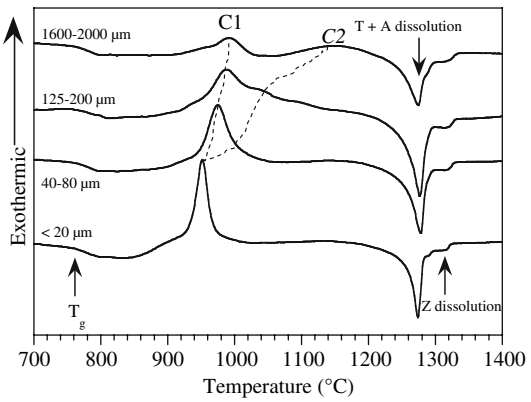

Fig. 4 DTA curves for different size fraction of GZr(Nd)$_c$ glass (heating rate :10 °C min^{-1}, weight ~ 200 mg). T: titanite, A: anorthite, Z: zirconolite. The onset used to determine T_g is also indicated. C1 and C2 are exothermic effects associated respectively to bulk and surface crystallization. The dotted lines are drawn as a guide for the eye to indicate the evolution of C1 and C2 peaks

broadened by second-order quadrupolar interaction and distribution of NMR parameters but recording the spectrum at relatively high field (14.1 T) and high spinning speed (26 kHz) in this study permits to limit the possible superposition between 4-, 5- and 6-fold coordinated Al sites. It can be noticed that the shape of the spectrum is asymmetric with a steep flank at low field side (high ppm values) and a more gradually decreasing high field side. Such a feature is characteristic of the existence of distribution of quadrupolar coupling constant C_Q, which is to be expected in glasses due to distribution of bonding distances and bonding angles [50, 51]. Study of GZr glass by ^{27}Al 3QMAS NMR (spectrum not shown) confirms that aluminum is only located in $(AlO_4)^-$ tetrahedral units. The glass containing Nd^{3+} ions (GZr(Nd)$_a$) shows relatively similar spectrum (Fig. 3b) but its shape is slightly broadened presumably because of the existence of interactions between aluminum nuclei and paramagnetic neodymium ions. Thus, for GZr and GZr(Nd)$_a$ glasses, aluminum enters glass network in 4-fold coordination suggesting that modifier cations (Na^+,Ca^{2+}) are present in sufficient amount to charge compensate the negative $(AlO_4)^-$ entities. Indeed, the molar ratio C = ([CaO] + [Na_2O])/[Al_2O_3] = 3.11 > 1 for GZr and GZr(Nd)$_a$ glasses (Table 1). As C remains higher than 2 for all glasses (C = 4.83 and 2.30 respectively for GZr(Nd)$_b$ and GZr(Nd)$_c$ glasses), calcium and sodium oxide contents are thus higher than the ones needed for ensuring a full charge compensation of $(AlO_4)^-$ entities. We can thus expect that aluminum occur in tetrahedral coordination in all glasses of this paper.

Crystallization study of GZr(Nd)$_c$ glass with DTA

Due to the high nucleation rate of zirconolite in the bulk of GZr(Nd)$_c$ glass (see below), DTA curves were recorded for this glass for different size fractions after grinding and sieving (Fig. 4). Indeed, due to the relatively low crystallization rate of zirconolite in GZr(Nd)$_a$ glass, the DTA exothermic effect associated with crystallization of zirconolite in the bulk was not detected for this composition [33]. Figure 4 shows the existence of two main exothermic effects C1 and C2 associated with crystallization. These two effects occur in the same temperature range for the smallest particle size (<20 µm) but become separated for higher particle sizes. The evolution of the position of the exothermic peaks temperature T_p with particle size is reported in Fig. 5. It appears that peak C1 is narrower than peak C2. Moreover, the enlargement and displacement of C2 towards high temperatures for higher particle sizes indicates that the corresponding effect is associated with

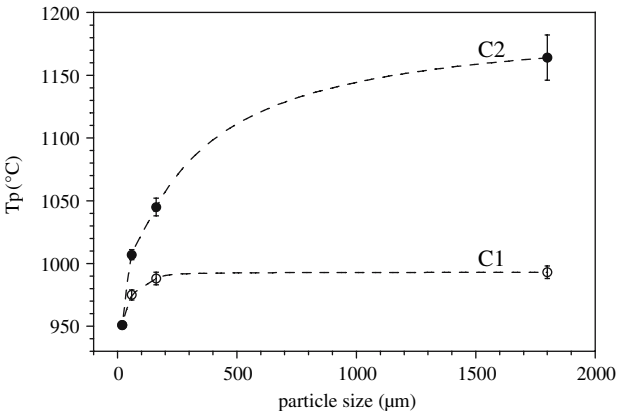

Fig. 5 Evolution of the position of exothermic DTA peaks (T_p) C1 (○) and C2 (●) with size fraction (GZr(Nd)$_c$ glass) from Fig. 4. The mean value of each size fraction is reported on the abscissa axis except for the size fraction <20 µm for which the value of 20 µm is reported. The errors bars associated with the data points are shown in the figure. The dotted lines drawn in the figure are given as a guide for the eye to show to the evolution of T_p for C1 and C2 peaks

surface crystallization. Indeed, it is known that T_p increases with glass particle size for crystallization regulated by surface nucleation [52, 53]. The fact that peak C1 is only slightly displaced towards high temperatures indicated that the corresponding effect is mainly due to internal crystallization (bulk nucleation). In order to identify the nature of the crystalline phases formed at T_p(C1) and T_p(C2), heat treatments were performed on the size fractions <20 μm and 125–200 μm at the corresponding T_p values for 10 min (heating rate: 10 °C min^{-1}). XRD patterns of the quenched samples were then recorded (Fig. 6). The study of these patterns shows that:

- C1 is associated with the crystallization (mainly in the bulk) of a defect-fluorite phase, which corresponds to a totally cationic disordered zirconolite (cubic structure). The crystallization of this phase was already observed in (ZrO_2, TiO_2)-rich glass compositions derived from GZr(Nd)$_a$ glass and was shown to transform irreversibly into the zirconolite-2M polytype (monoclinic structure) at higher temperature [33]. Figure 6b, c shows that partial transformation of defect-fluorite crystals into zirconolite crystals occurs between the two peaks C1 and C2.
- C2 is associated with the crystallization of titanite + anorthite. These silicate phases were shown previously to nucleate heterogeneously on glass surface [33]. This is in accordance with the evolution observed on DTA curves when the particle size increases (Fig. 4).

Consequently, the high nucleation rate I_Z of zirconolite (or more precisely of its disordered fluorite-defect precursor) in the bulk of GZr(Nd)$_c$ glass enables the detection of an exothermic effect associated with the crystallization of this phase. This was not the case for GZr(Nd)$_a$ glass for which only the exothermic effects associated with the crystallization of titanite and anorthite from glass surface were observed [33]. Figure 4 also shows the endothermic effects (T > 1250 °C) associated with the dissolution of crystalline phases (titanite, anorthite, zirconolite) in the residual glass. Comparison with the results reported in [33] shows that the first endothermic effect occurring near 1275 °C is due to titanite + anorthite dissolution whereas the second endothermic effect near 1320 °C is probably associated with zirconolite dissolution.

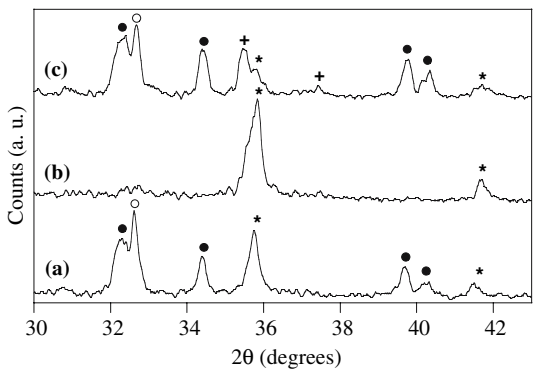

Fig. 6 XRD patterns (λCoK_α) of GZr(Nd)$_c$ glass heat treated: (**a**) up to 950 °C (T_p(C1) = T_p(C2)) for the size fraction <20 μm; (**b**) up to 990 °C (T_p(C1)) for the size fraction 125–200 μm; (**c**) up to 1045 °C (T_p(C2)) for the size fraction 125–200 μm. Heating rate 10 °C. min^{-1}. The samples were kept for 10 min at the corresponding temperature and were then quenched to room temperature. (●: titanite, ○: anorthite, ⁎: defect-fluorite phase, + : zirconolite-2M)

Study of glass-ceramics

The glass-ceramics obtained after nucleation (810 °C, 2 h) + crystal growth (1050 °C or 1200 °C, 2 h) were mainly studied by SEM, EDX and XRD. The results concerning GZr(Nd)$_a$ glass were already presented and discussed in [17–19, 33]. In this paper, we will compare the results obtained for the compositions derived from GZr(Nd)$_a$ and GHf(Nd)$_a$ by increasing or decreasing Al_2O_3 concentration. The nature of crystalline phases formed in the bulk or near sample surface (crystallized layer) at T_c = 1050 °C and 1200 °C for all glasses are summarized in Table 2.

Glass-ceramics with ZrO_2

Heat treatment of GZr(Nd)$_b$ sample at T_c = 1050 °C or 1200 °C leads to the formation of a surface crystallized layer constituted of only titanite crystals (Fig. 7). Contrary to GZr(Nd)$_a$ sample (Fig. 8a), anorthite crystallization is not observed in GZr(Nd)$_b$ sample. The lack of anorthite in this glass after heat treatment can be explained by the decrease of the crystallization driving force of this phase when Al_2O_3 concentration decreases. Indeed, Al_2O_3 is one of the main oxides constituting anorthite and if we consider only CaO, Al_2O_3 and SiO_2, the GZr(Nd)$_a$ glass composition is located on the boundary between anorthite

Table 2 Nature of crystalline phases formed in the bulk or near sample surface (crystallized layer) after heat treatment at T_n = 810 °C (2 h) and T_c = 1050 °C or 1200 °C (2 h) for the glasses studied in this work

Glass	Bulk		Surface	
	1050 °C	1200 °C	1050 °C	1200 °C
GZr(Nd)$_a$	Z	Z	T + A	T + A + B
GZr(Nd)$_b$	no crystals	no crystals	T	T
GZr(Nd)$_c$	Z	Z + A	T + A	T + A + B + Z
GHf(Nd)$_a$	Z	Z	T + A	T + A
GHf(Nd)$_c$	Z	T + A	T + A	T + A

Z: zirconolite; T: titanite; B: baddeleyite; A: anorthite

and pseudo-wollastonite primary crystallization fields in the SiO_2–Al_2O_3–CaO phase diagram [54]. Thus, the decrease of Al_2O_3 concentration (from GZr(Nd)$_a$ to GZr(Nd)$_b$ composition) displaces glass composition away from the anorthite crystallization field on the phase diagram and the crystallization driving force of this phase decreases. Moreover, the bulk of GZr(Nd)$_b$ sample remains totally amorphous after heat treatment at T_c = 1050 °C or 1200 °C. Contrary to the results obtained for GZr(Nd)$_a$ glass (Fig. 8b), zirconolite crystallization is thus not observed in the bulk of this sample indicating a strong decrease of I_Z. Considerations about the increasing availability of charge compensators (Ca^{2+} and Na^+ cations) when Al_2O_3 concentration decreases can explain this striking result. Indeed, we showed above by MAS NMR that all Al^{3+} ions were stabilized as charge compensated $(AlO_4)^-$ entities in the structure of GZr and GZr(Nd)$_a$ glasses. Moreover, it is known that in silicate glasses containing sufficient charge compensators, Zr^{4+} and Ti^{4+} ions can be stabilized in respectively 6-fold and 5-fold coordination as ZrO_6 octahedra [44, 55] and TiO_5 square base pyramids with a short titanyl non bridging bond and four Ti–O–Si bonds [56–58]. In this case, the negative charge excess (–2) of zirconium and titanium polyhedra is locally compensated by modifier cations. Thus, in the glass system studied in this paper, a competition is expected between Al^{3+}, Zr^{4+} and Ti^{4+} ions for their association with modifier cations Ca^{2+} and Na^{2+} to balance the local charge deficit of polyhedra. For instance, if we consider the total concentration of CaO and Na_2O in GZr glass, it appears that there is only a slight excess S of modifier oxides available to form NBO after charge compensation of both aluminum, zirconium and titanium polyhedra in glass structure (S = [Na_2O] + [CaO]–[Al_2O_3]–[TiO_2]–[ZrO_2] = + 1.7 mol%, assuming that Na^+ and Ca^{2+} ions compensate the negative charge excess of $(AlO_4)^-$, $(O = TiO_4)^{2-}$ and $(ZrO_6)^{2-}$ entities [44, 56, 57]). Consequently, by decreasing Zr^{4+} and Ti^{4+} ions activities, the increase of modifiers concentration would facilitate zirconium and titanium dissolution in the glass structure and in the undercooled melt at T_n. The decrease of Al_2O_3 concentration in GZr(Nd)$_b$ glass composition in comparison with GZr(Nd)$_a$ is thus expected to increase the amount of modifiers available for the stabilization of Zr^{4+} and Ti^{4+} ions in the glass (for this composition S = + 4.78 mol%). As ZrO_2 and TiO_2 are (with CaO) the constituents of

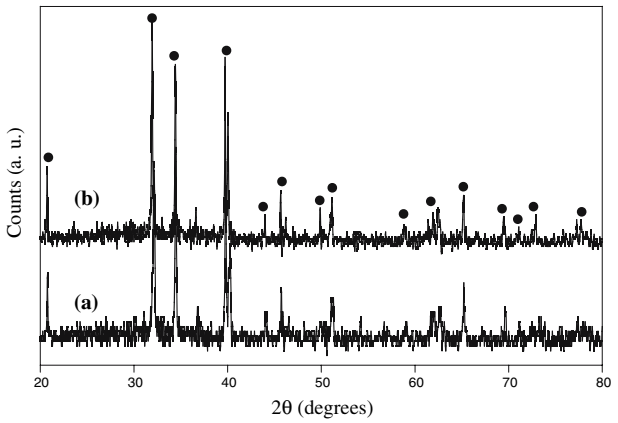

Fig. 7 XRD pattern (λCoK_α) of the surface crystallized layer of GZr(Nd)$_b$ sample heat treated at T_c = 1050 °C (**a**) and T_c = 1200 °C (**b**). (●: titanite)

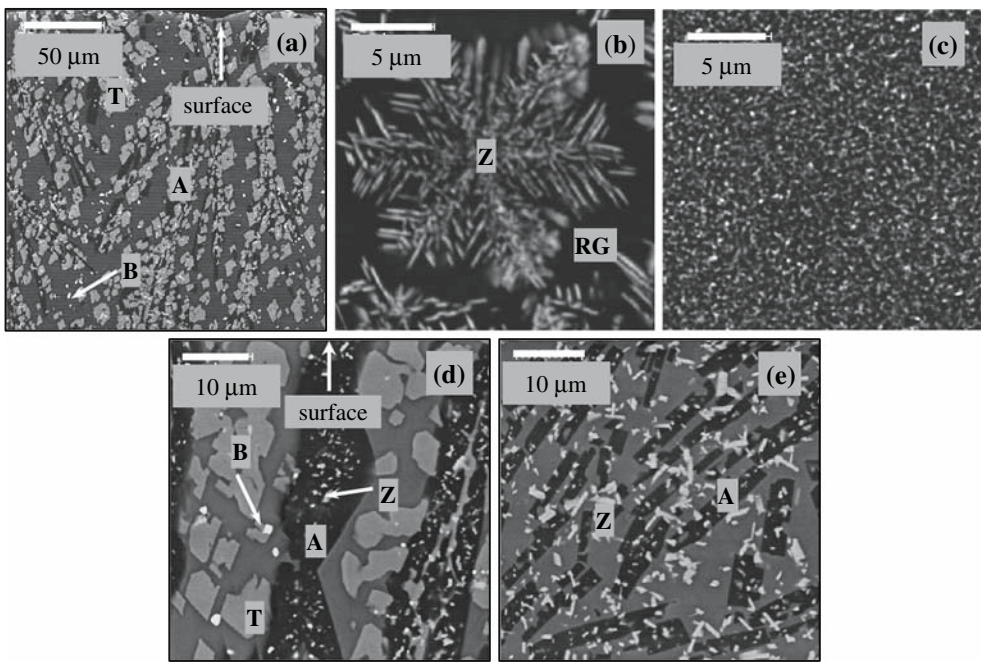

Fig. 8 Back-scattered SEM micrographs of the: (**a**) surface of GZr(Nd)$_a$ glass heat treated at T_c = 1200 °C; (**b**) bulk of GZr(Nd)$_a$ glass heat treated at T_c = 1050 °C; (**c**) bulk of GZr(Nd)$_c$ glass heat treated at T_c = 1050 °C; (**d**) surface of GZr(Nd)$_c$ glass heat treated at T_c = 1200 °C; (**e**) bulk of GZr(Nd)$_c$ glass heat treated at T_c = 1200 °C. All samples were nucleated at T_n = 810 °C for 2 h. Due to the lack of heavy elements (Zr, Nd) in its structure, anorthite appears in dark on the images. (A: anorthite, T: titanite, Z: zirconolite, B: baddeleyite). The continuous gray (**a**, **d**, **e**) or black (**b**) phase corresponds to residual glass (RG). The size of the white scales is indicated in the figure

zirconolite, a decrease of Al_2O_3 concentration would thus induce a decrease of the crystallization driving force of zirconolite. This could explain the lack of zirconolite nucleation in the bulk of GZr(Nd)$_b$ sample after heat treatment. Moreover, it is interesting to underline that contrary to GZr(Nd)$_a$ glass (Fig. 8a) [33], baddeleyite (nominally ZrO_2) crystallization is not detected in the surface crystallized layer of GZr(Nd)$_b$ sample at T_c = 1200 °C (Fig. 7). This result could be also explained by the increase of zirconium solubility in the glass due to the increase of modifier cations amount available to charge compensate $(ZrO_6)^{2-}$ entities when Al_2O_3 concentration decreases.

For GZr(Nd)$_c$, a thin crystallized layer (80–100 μm) constituted of titanite and anorthite is formed at T_c = 1050 °C whereas a very high number of zirconolite crystals nucleate and grow in the bulk (Fig. 8c). Comparison of Fig. 8b, c clearly shows strong increase of I_Z between GZr(Nd)$_a$ and GZr(Nd)$_c$ compositions. This confirms the tendency observed above between GZr(Nd)$_a$ and GZr(Nd)$_b$ compositions. The negative value S = –1.25 mol% calculated from GZr(Nd)$_c$ composition shows that Ca^{2+} and Na^+ cations are not sufficient to fully compensate the local charge deficit of both $(AlO_4)^-$, $(ZrO_6)^{2-}$ and $(TiO_5)^{2-}$ entities. If we admit that aluminum competes favorably with zirconium and titanium for charge compensators and remains as $(AlO_4)^-$ entities as long as C > 1, the increase of Al_2O_3 concentration from 5.57 to 11.00 mol% would destabilizes $(ZrO_6)^{2-}$ and $(TiO_5)^{2-}$ entities and would thus increase zirconium + titanium activities and I_Z. At T_c = 1200 °C, a thick crystallized layer (~2 mm) constituted of titanite, anorthite, baddeleyite and zirconolite is observed near GZr(Nd)$_c$ sample surface (Fig. 8d). The zirconolite crystals observed in this layer have nucleated in the bulk and were then trapped in the layer because of the high growth rate of titanite and anorthite crystals from sample surface. At T_c = 1200 °C, the bulk of the glass-ceramic contains zirconolite and anorthite crystals (Fig. 8e). The anorthite crystals in the bulk have grown from glass surface towards the bulk and are present in the whole centimeter size sample. Thus, in comparison with GZr(Nd)$_a$, the crystal growth rate of anorthite strongly increases for GZr(Nd)$_c$. This effect is due to the increase of the Al_2O_3 amount available in the system. In order to obtain a glass-ceramic containing only zirconolite crystals in its bulk at T_c = 1200 °C, the duration of the crystal growth must be decreased ($t \ll 2$ h) for GZr(Nd)$_c$. As both zirconolite nucleation and crystal growth rates are very high for this composition, keeping the nucleated sample a few minutes at T_c = 1200 °C would be probably sufficient to obtain such a glass-ceramic. The crystallization of baddeleyite in the surface layer at T_c = 1200 °C confirms the decrease of ZrO_2 solubility in the glass and in the undercooled melt when Al_2O_3 concentration increases.

Table 3 Formula of titanite and zirconolite crystals formed respectively near the surface and in the bulk of GZr(Nd)$_c$ and GZr(Nd)$_a$ glasses heat treated at T_c = 1200 °C determined by EDX

T_c = 1200 °C	GZr(Nd)$_c$	GZr(Nd)$_a$
Titanite (surface)	$Ca_{0.88}Nd_{0.12}Ti_{0.72}Zr_{0.21}Al_{0.12}Si_{0.95}O_5$	$Ca_{0.89}Nd_{0.11}Ti_{0.69}Zr_{0.22}Al_{0.11}Si_{0.98}O_5$
Zirconolite (bulk)	$Ca_{0.82}Nd_{0.19}Zr_{1.04}Ti_{1.78}Al_{0.17}O_7$	$Ca_{0.82}Nd_{0.19}Zr_{1.05}Ti_{1.77}Al_{0.17}O_7$

Nucleation heat treatment: Tn = 810 °C, 2 h

The composition of the crystalline phases able to incorporate Nd^{3+} ions (titanite, zirconolite) was determined by EDX for the GZr(Nd)$_c$ glass-ceramic prepared at T_c = 1200 °C (Table 3). At this temperature the crystals were thick enough to be probed by the electron beam. For comparison, the composition of the titanite and zirconolite crystals formed respectively near the surface and in the bulk of GZr(Nd)$_a$ glass heat treated at T_c = 1200 °C is also given in Table 3. It appears that increasing Al_2O_3 concentration in GZr(Nd)$_a$ glass has not significant effect on the composition of zirconolite and titanite crystals. Nd^{3+} ions enter in the calcium site of these phases with charge compensation mainly insured by Al^{3+} ions. Thus, increasing alumina concentration in parent glass does not enable the incorporation of a higher amount of neodymium oxide into zirconolite crystals. This result is probably due to the simultaneous crystallization of anorthite in the bulk of GZr(Nd)$_c$ glass that consumes an important fraction of Al_2O_3 (Fig. 8e).

Using ESR and the quantitative method developed in [37], the neodymium partitioning ratio R in zirconolite (i.e. the molar fraction of Nd^{3+} ions incorporated into the zirconolite phase) was determined for the bulk of GZr(Nd)$_a$ and GZr(Nd)$_c$ glass-ceramics (Table 4). In accordance with previous results published in [37], it is clear that R decreases when the crystal growth temperature increases. Different origins were proposed to explain this evolution [37]. A slight increase of R by 4% is observed between GZr(Nd)$_a$ and GZr(Nd)$_c$ glass-ceramics at T_c = 1050 °C. This evolution could be due both to the increase of the

Table 4 Partitioning ratio R of neodymium ions between zirconolite crystals and the residual glass in the bulk of GZr(Nd)$_a$ and GZr(Nd)$_c$ glasses heat treated at T_c = 1050 °C or 1200 °C (2 h) after nucleation step at T_n = 810 °C (2 h)

R	T_c = 1050 °C (2 h)	T_c = 1200 °C (2 h)
GZr(Nd)$_a$	36 %	24 %
GZr(Nd)$_c$	40 %	37 %

R was determined by ESR according to the method described in [37] (estimated errors in the values of R ± 2%)

amount of zirconolite crystals in the bulk (compare Fig. 8b, c) and/or to the increase of the amount of neodymium incorporated into zirconolite crystals by formula unit. However, due to the small crystals size at T_c = 1050 °C, their composition remains unknown. At T_c = 1200 °C, R increases from 24% to 37% between GZr(Nd)$_a$ and GZr(Nd)$_c$ samples. This evolution cannot be attributed to neodymium concentration increase in zirconolite because crystals composition does not significantly change when Al_2O_3 concentration increases (Table 3). Consequently, it is only the increase of the amount of zirconolite crystals in the bulk of GZr(Nd)$_c$ glass-ceramic prepared at T_c = 1200 °C that can explain the increase of R.

Glass-ceramics with HfO_2

Comparison of Fig. 9a, c shows that total substitution of zirconium by hafnium in GZr(Nd)$_a$ composition (giving GHf(Nd)$_a$ composition, Table 1) induces a significant decrease of I_Z. This result is in accordance with the nucleation rate curves $I_Z = f(T)$ of zirconolite in the bulk of GZr(Nd)$_a$ and GHf(Nd)$_a$ glasses presented in [34, 59] where it was shown that the maximum of the nucleation rate curve decreased by approximately three orders of magnitude for the sample containing hafnium. Considerations—that will be not presented here—about both solubility and diffusion coefficient differences between Hf^{4+} and Zr^{4+} ions in glasses and melts were developed in [34, 59] to try to explain the lower nucleation rate of zirconolite in glasses containing hafnium. The composition of zirconolite crystals formed at T_c = 1200 °C in the bulk of GHf(Nd)$_a$ glass (Fig. 9b) was determined by EPMA ($Ca_{0.85}Nd_{0.21}Hf_{1.08}Ti_{1.71}Al_{0.18}O_7$). This composition is close to that of zirconolite crystals formed at T_c = 1200 °C in the bulk of GZr(Nd)$_a$ glass (Table 3). This shows that nearly the same amount of neodymium (by zirconolite formula unit) was incorporated into the crystals for the two samples and that charge compensation was mainly ensured by Al^{3+} ions in titanium sites. This result also demonstrates that high amount of neutron poison (hafnium) can be incorporated simultaneously with trivalent actinides surrogate into zirconolite crystals after heat treatment of GHf(Nd)$_a$ glass. Nevertheless, ESR shows that for this sample heat treated at T_c = 1200 °C (Fig. 9b), the partitioning ratio R of neodymium between zirconolite and residual glass only reaches R = 21% whereas under the same heat treatment conditions R = 24% for GZr(Nd)$_a$ sample. This difference can be explained by the smaller number of zirconolite nuclei formed during nucleation step for GHf(Nd)$_a$ sample.

According to the composition change effects observed above on I_Z for glasses containing zirconium, Al_2O_3 concentration was raised by approximately 3 wt% in GHf(Nd)$_a$ parent glass in order to increase I_Z (GHf(Nd)$_c$ composition, Table 1). The SEM images of the bulk of GHf(Nd)$_c$ glass-ceramics prepared at T_c = 1050 °C and 1200 °C are shown respectively in Fig. 9d, e. A strong increase of I_Z—by nearly three orders of magnitude—is observed between GHf(Nd)$_a$ and GHf(Nd)$_c$ samples (compare Fig. 9a, d, T_c = 1050 °C) and the number of zirconolite crystals formed in the bulk of GHf(Nd)$_c$ and GZr(Nd)$_a$ glasses after crystal growth at T_c = 1050 °C are close (compare Fig. 9c, d). Similarly to the discussion developed above for glasses with zirconium, the effect of increasing Al_2O_3 concentration on I_Z for glasses with hafnium can be attributed to the increase of Hf^{4+} and Ti^{4+} activities in undercooled melt due to the existence of a competition between Al^{3+} and (Hf^{4+}, Ti^{4+}) ions to associate with charge compensators to stabilize $(AlO_4)^-$, $(O = TiO_4)^{2-}$ and $(HfO_6)^{2-}$ entities (S = –1.25 mol% for GHf(Nd)$_c$ sample). Consequently, we propose that the increase of Al_2O_3 concentration would destabilize (Hf^{4+}, Ti^{4+}) ions in the undercooled melt and would thus increase I_Z.

Concerning the crystal growth heat treatment at T_c = 1200 °C (2 h), Fig. 9e shows that the bulk of GHf(Nd)$_c$ glass-ceramic contains only titanite + anorthite crystals that have grown from sample surface (no zirconolite crystals were detected in the bulk). These results are thus different to those of GZr(Nd)$_c$ sample for which only zirconolite and anorthite crystals were observed in the bulk at T_c = 1200 °C (Fig. 8e). The lack of titanite in the bulk of GZr(Nd)$_c$ sample was probably due to the high amount of zirconolite crystals nucleating and growing in the bulk (Fig. 8e) and that slowed down the growth rate of titanite crystals (titanite nucleates only on glass surface [21]). We propose that, at T_c = 1200 °C, the presence of zirconolite crystals in GZr(Nd)$_c$ sample strongly reduce titanite crystals growth rate because of the strong decrease of TiO_2 concentration in residual glass (titanium is one of the main constituents of both titanite and zirconolite phases). For GHf(Nd)$_c$ sample, the small number of zirconolite nuclei formed after nucleation could explain the higher growth rate of titanite crystals.

Consequently, for the waste form application envisaged in this study, Al_2O_3 concentration in GHf(Nd)$_a$ parent glass can be raised in order to increase I_Z. However, contrary to the sample with zirconium, the crystal growth temperature T_c must remain relatively low (for instance T_c = 1050 °C) in order to avoid the growth of titanite in the bulk at the expenses of zirconolite (Fig. 9e).

Conclusions

Glass-ceramics containing zirconolite (nominally $Ca(Zr,Hf)Ti_2O_7$) crystals in their bulk that would incor-

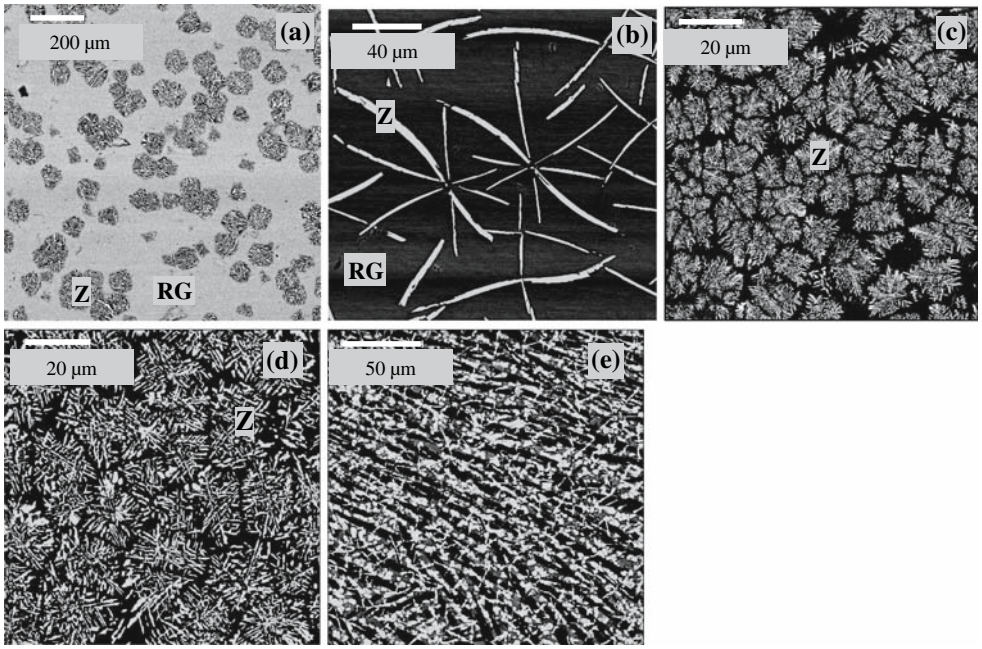

Fig. 9 Back-scattered SEM micrographs of the bulk of: (**a**) $GHf(Nd)_a$ glass-ceramic heat treated at T_c = 1050 °C (2 h); (**b**) $GHf(Nd)_a$ glass-ceramic heat treated at T_c = 1200 °C (2 h); (**c**) $GZr(Nd)_a$ glass-ceramic heat treated at T_c = 1050 °C (2 h); $GHf(Nd)_c$ glass-ceramic heat treated at T_c = 1050 °C (2 h) (**d**) or at T_c = 1200 °C (2 h) (**e**). All the samples were nucleated at T_n = 810 °C for 2 h. In (b,c,d) and (**a**) the residual glass between zirconolite crystals appears in black and grey respectively. This contrast difference shows that in (**b**, **c**, **d**) zirconolite strongly depletes residual glass in heavy elements (zirconium) whereas in (**a**) the size and the number of zirconolite crystals were not high enough to deplete residual glass in heavy elements in residual between them. In (**e**) no zirconolite crystals were detected, the black and white crystals correspond respectively to anorthite and titanite whereas the grey phase corresponds to residual glass. (Z: zirconolite, A: anorthite, T: titanite, RG: residual glass). The size of the white scales is indicated in the figure. It is important to notice the different scale bars between micrographs

porate high proportions of minor actinides or plutonium could be envisaged as matrices for these wastes. In this study, we performed composition changes by decreasing or increasing Al_2O_3 content in SiO_2–Al_2O_3–CaO–Na_2O–TiO_2 parent glasses containing either ZrO_2 or HfO_2. Neodymium was used as trivalent minor actinides and plutonium surrogate. The main conclusions that can be drawn concerning the structure and the crystallization behavior of these glasses are the following:

(i) Optical absorption and fluorescence study of parent glasses showed that the environment of Nd^{3+} ions was not significantly affected by total substitution of Zr by Hf or by changing Al_2O_3 content. ^{27}Al MAS NMR showed that aluminum enters GZr and $GZr(Nd)_a$ parent glasses network predominantly in 4-fold coordination.

(ii) Zirconolite crystals formed in the bulk of glass-ceramics prepared by nucleation (T_n = 810 °C, 2 h) and crystal growth (T_c = 1050° or 1200 °C, 2 h) steps was followed for all glass compositions (Table 2). It appeared that decreasing Al_2O_3 concentration by 2.8 mol% in glass containing ZrO_2 strongly reduced zirconolite nucleation rate I_Z in the bulk and titanite (nominally $CaTiSiO_5$) was the only crystalline phase growing from glass surface towards bulk at T_c. However, I_Z strongly increased when Al_2O_3 concentration was raised by 2.6 mol% in glasses containing ZrO_2 or HfO_2. When crystal growth temperature T_c = 1050 °C, zirconolite was the only crystalline phase in the bulk. However, at T_c = 1200 °C, (anorthite + zirconolite) or (anorthite + titanite) crystals were observed in the bulk of glass-ceramics containing respectively ZrO_2 or HfO_2. The strong effect of Al_2O_3 concentration on I_Z could be explained considering the existence of a competition between Al^{3+} ions and (Ti^{4+}, Zr^{4+}, Hf^{4+}) ions for association with charge compensators (Ca^{2+}, Na^+) to stabilize $(AlO_4)^-$, $(ZrO_6)^{2-}$, $(HfO_6)^{2-}$ and $(TiO_5)^{2-}$ entities in glass structure.

(iii) Total substitution of Zr by Hf in parent glasses induced strong decrease of I_Z. Nevertheless, the composition of zirconolite crystals formed at T_c = 1200 °C in $GZr(Nd)_a$ and $GHf(Nd)_a$ glasses were very similar. Nearly the same amount of neodymium was incorporated into the crystals and charge compensation was mainly ensured by Al^{3+} ions. Moreover, ESR shows that—at least for the

samples heat treated at T_c = 1200 °C—the partitioning ratio R of neodymium between zirconolite and residual glass only decreased by 3% in sample containing hafnium. This study of glasses with HfO_2 demonstrates that high amount of neutron poison (hafnium) can be incorporated simultaneously with trivalent actinides surrogate into zirconolite crystals after heat treatment.

(iv) EDX analysis indicated that the composition of zirconolite crystals formed in glasses containing ZrO_2 (T_c = 1200 °C) did not depend on Al_2O_3 concentration. The majority of Nd^{3+} ions are incorporated into the calcium site of zirconolite structure and charge compensation is mainly insured by Al^{3+} ions into titanium sites. ESR indicated that raising Al_2O_3 concentration lead to increase R, which can be explained by the increase of the amount of zirconolite crystals in the bulk. Unfortunately, even for the highest Al_2O_3 concentration, only 40% and 37% of all Nd^{3+} ions in samples heat treated respectively at T_c = 1050° and 1200 °C benefit from a double containment barrier (zirconolite + residual glass) because of the high quantity of neodymium remaining in residual glass. Consequently, these R values remained too small to make realistic the use of the compositions studied in this work for the conditioning of minor actinides or plutonium. Nevertheless, other glass-ceramics containing apatite ($Ca_2Nd_8Si_6O_{26}$) crystals that are more efficient to concentrate neodymium than zirconolite crystals are currently under study in our laboratory as potential matrices to immobilize minor actinides or plutonium [21].

Acknowledgements The CEA (Commissariat à l'Energie Atomique) and the French Group Nomade are gratefully acknowledged for their financial supports to this study. The authors would like also to thank Prof. G. Bodenhausen (Ecole Normale Supérieure, Paris) who made possible the ^{27}Al MAS NMR experiment at 14.1 T. The authors also thank Dr. T. Charpentier and Dr. M. Gaillard (CEA Saclay, France) for recording of ^{27}Al 3QMAS NMR spectrum.

References

1. Lee WE, Ojovan MI, Stennet MC, Hyatt NC (2006) Adv Appl Ceram 105:3
2. Ojovan MI, Lee WE (2005) An introduction to nuclear waste immobilisation. Elsevier, Oxford, UK
3. Donald IW, Metcalfe BL, Taylor RNJ (1997) J Mater Sci 32:5851
4. Caurant D, Loiseau P, Aubin-Chevaldonnet V, Gourier D, Majérus O, Bardez I, In: Keister JE (ed) Nuclear Materials Research Developments, Ceramics, Glass-Ceramics And Glasses For Immobilization Of High-Level Nuclear Wastes. Nova Science Publishers, Hauppauge, NY, USA (In Press)
5. Guillaumont R (2004) C R Chimie 7:1129
6. Fillet C, Advocat T, Bart F, Leturcq G, Rabiller H (2004) C R Chimie 7:1165
7. Guy C, Audubert F, Lartigue J-E, Latrille C, Advocat T, Fillet C (2002) C R Physique, 3:827
8. Dacheux N, Clavier N, Robisson A-C, Terra O, Audubert F, Lartigue J-E, Guy C (2004) C R Chimie 7:1141
9. Aubin-Chevaldonnet V, Caurant D, Dannoux A, Gourier D, Charpentier T, Mazerolles L, Advocat T (2007) J. Nucl. Mater. 366:137
10. Madic C, Lecomte M, Baron P, Boullis B (2002) C R Physique 3:797
11. Boullis B (2002) Clefs Cea 46:18
12. Ochkin AV, Stefanovsky SV, Rovny SI (2003) Mat Res Soc Symp Proc 757:315
13. Ochkin AV, Stefanovsky SV, Ptashkin AG, Mikhailenko NS, Kirjanova OI (2004) Mat Res Soc Symp Proc 824:267
14. Boullis B (1997) In: Turlay R (ed) Société Française De Physique, Les Editions De Physique. Les Ullis, France, p 69
15. Soulet S, Carpena J, Chaumont J, Kaitasov O, Ruault M-O, Krupa J-C (2001) Nucl Instrum Meth B 184:383
16. Yudinstev SV (2003) Geol Ore Deposits 45:151
17. Loiseau P, Caurant D, Majérus O, Baffier N, Fillet C (2003) J Mater Sci 38:843
18. Loiseau P, Caurant D, Majérus O, Baffier N, Mazerolles L, Fillet C (2002) Phys Chem Glasses 43C:195
19. Loiseau P, Caurant D, Baffier N, Mazerolles L, Fillet C (2001) Mat Res Soc Symp Proc 663:179
20. Loiseau P, Caurant D, Majérus O, Baffier N, Fillet C (2004) Mat Res Soc Symp Proc 807:333
21. Caurant D, Majérus O, Loiseau P, Bardez I, Baffier N, Dussossoy JL (2006) J Nucl Mater 354:143
22. Loiseau P, Phd Thesis, Université Paris VI (France), 2001
23. Loiseau P, Caurant D, Baffier N, Mazerolles L, Fillet C (2004) J Nucl Mater 335:14
24. Fielding PE, White TJ (1987) J Mater Res 2:387
25. Loiseau P, Caurant D, Baffier N, Fillet C (2003) Mat Res Soc Symp Proc 757:243
26. Rossell HJ (1992) J Solid State Chem 99:38
27. Begg PD, Vance ER, Day RA, Hambley M, Conradson SD (1997) Mat Res Soc Symp Proc 465:325
28. Jorion F, Deschanels X, Advocat T, Desmouliere F, Cachia JN, Peuget S, Roudil D, Leturcq G (2006) Nucl Sci Eng 153:262
29. Leturcq G, Mcglinn PJ, Barbe C, Blackford MG, Finnie KS (2005) Appl Geochem 20:899
30. Mcglinn PJ, Advocat T, Leturcq G, Mcleod TI, Aly Z, Yee P (2006) Mat Res Soc Symp Proc 932:575
31. Smith KL, Zhang Z, Mcglinn P, Attard D, Li H, Lumpkin GR, Colella M, Mcleod T, Aly Z, Loi E, Leung S, Hart KP, Ridgway M, Weber WJ, Thevuthasan S (2003) Mat Res Soc Symp Proc 757:289
32. Smith KL, Lumpkin GR (1993) In: Boland JN, And Fitzgerald JD (eds) defects and processes in the solid state: geoscience applications. Elsevier, Amsterdam, Netherlands, p. 401
33. Loiseau P, Caurant D, Majérus O, Baffier N, Fillet C (2003) J Mater Sci 38:853
34. Loiseau P, Caurant D, Bardez I, Majérus O, Baffier N, Fillet C (2003) Mat Res Soc Symp Proc 757:281
35. Loiseau P, Caurant D, Baffier N, Fillet C (2003) Phys Chem Glasses 43C:201
36. Man PP (1993) Mol Phys 78:307
37. Loiseau P, Caurant D, Baffier N, Fillet C (2001) Mat Res Soc Symp Proc 663:169
38. Dymnikov AA, Przhevuskii AK (1997) J Non-Cryst Solids 215:83
39. Gatterer K (1997) In: Wright AC, Feller SA, And Hannon AC (eds) Borates glasses, crystals and melts. Alden, Oxford, UK, p 384
40. Gatterer K, Pucker G, Jantscher W, Fritzer HP, Arafa S (1998) J Non-Cryst Solids 231:189

41. Bardez I, Caurant D, Loiseau P, Baffier N, Dussossoy JL, Gervais C, Ribot F, Neuville DR (2005) Phys Chem Glasses 46:320
42. Quintas A, Majérus O, Lenoir M, Caurant D, Klementiev K, Webb A, Dussossoy J-L, J Non-Cryst Solids (In Press)
43. Viana B, Lejus AM, Saber D, Duxin N, Vivien D (1994) Opt Mater 3:307
44. Galoisy L, Pelegrin E, Arrio M-A, Ildefonse P, Calas G (1999) J Am Ceram Soc 82:2219
45. Caulder DL, Booth CH, Bucher JJ, Edelstein NM, Liu P, Lukens WW, Rao L, Shuh DK, Davis LL, Darab JG, Li H, Li L, Strachan DMs, 219th American chemical society national meeting. Division of nuclear chemistry and technology. Symposium on nuclear waste remediation and long term storage. San Francisco, 26–30 March 2000 (Poster Session)
46. Engelhardt G, Michel D (1987) In: High resolution solid-state Nmr in silicates and zeolites. Wiley, NewYork
47. Smith ME (1993) Appl Magn Reson 4:1
48. Stebbins JF (1995) In: Ahrens TJ (ed) Handbook Of Physical Constants 2. American Geophysical Union, Washington D.C., p 303
49. Jäger C (1999) In: Bach H, Krause D (eds) Analysis of the composition and structure of glass and glass ceramics. Springer-Verlag, Berlin, Germany, p 197
50. Kentgens APM (1997) Geoderma 80:271
51. Ollier N, Charpentier T, Boizot B, Petite G (2004) J Phys Condens Matter 16:7625
52. Koga N, Sestak J, Strnad Z (1992) Thermochim Acta 203:361
53. Xu XJ, Ray CS, Day DE (1991) J Amer Ceram Soc 74:909
54. Osborn EF, Muan A (1964) In: Phase Diagrams For Ceramists. The American Ceramic Society, Columbus, Oh, p 219
55. Farges F, Ponader CW, Brown GE (1991) Geochim Cosmochim Acta 55:1563
56. Cormier L, Calas G, Gaskell PH (1997) J Phys Condens Matter 9:10129
57. Galoisy L, Cormier L, Rossano S, Ramos A, Calas G, Gaskell P, Le Grand M (2000) Mineral Mag 64:207
58. Cormier L, Gaskell PH, Calas G, Zhao J, Soper AK (1997) Physica B 234–236:393
59. Caurant D, Bardez I, Loiseau P (Submitted To J Mater Sci)